Acta Cryst. (1993). B49, 497–506

Phase Transitions of the Halogen-Bridged M^{II}—X—M^{IV} Mixed-Valence Complexes $[M(en)_2][MX_2(en)_2](ClO_4)_4$ (M = Pt, Pd; X = Cl, Br). Structural Studies of the High- and Low-Temperature Phases of $[Pt(en)_2][PtBr_2(en)_2](ClO_4)_4$

BY KOSHIRO TORIUMI*

Institute for Molecular Science, Okazaki National Research Institutes, Okazaki 444, *Japan*

MASAHIRO YAMASHITA

Department of Chemistry, College of General Education, Nagoya University, Chikusa-ku, Nagoya 464, *Japan*

SUSUMU KURITA

Laboratory of Applied Physics, Faculty of Engineering, Yokohama National University, Hodogaya, Yokohama 240, *Japan*

ICHIRO MURASE

Laboratory of Chemistry, College of General Education, Kyushu University, Ropponmatsu, Fukuoka 810, *Japan*

AND TASUKU ITO

Department of Chemistry, Faculty of Science, Tohoku University, Aoba Aramaki, Sendai 980, *Japan*

(*Received* 12 *July* 1990; *accepted* 7 *September* 1992)

Abstract

Halogen-bridged M^{II}—X—M^{IV} mixed-valence complexes $[M(en)_2][MX_2(en)_2](ClO_4)_4$ (M = Pt, Pd; X = Cl, Br; en = ethylenediamine) with linear-chain structures exhibit first-order phase transitions within the temperature range 269–298 K. The temperature dependence of the lattice parameters along the linear chains revealed discontinuous but reversible changes with negative thermal expansions at the phase-transition temperatures. The crystal structures of the orthorhombic (high-temperature) and monoclinic (low-temperature) phases of $[Pt(en)_2][PtBr_2(en)_2](ClO_4)_4$ have been determined by X-ray diffraction methods at room temperature. Both structures consist of infinite linear chains with a $\cdots Pt^{II}\cdots Br—Pt^{IV}—Br\cdots$ repeating unit along the b axes. It has been revealed that the conformations of the ethylenediamine chelate rings of the $Pt(en)_2$ moieties are changed on phase transition from $\lambda\lambda$ ($\delta\delta$) in the orthorhombic form to $\delta\lambda$ ($\lambda\delta$) in the monoclinic form. A change in the molecular symmetry as a result of the conformational change corresponds to the change in site symmetry at the Pt complex from 222 to $\bar{1}$. Structural differences can be explained by the sequences of the chelate-ring conformations in the chains, with repeating units of $[(\lambda\lambda)(\delta\delta)]$ for the orthorhombic and $[(\delta\lambda)(\lambda\delta)]$ for the monoclinic form, the conformations being coupled with each other through intra- and inter-chain NH···O(perchlorate)···HN hydrogen bonds. The hydrogen-bond network is also changed as a result of the conformational change from a three-dimensional structure (orthorhombic) to a two-dimensional one (monoclinic). The X-ray structure analyses also revealed that both the Pt^{IV}—Br and $Pt^{II}\cdots$Br distances in the monoclinic phase are significantly elongated when compared with those in the orthorhombic phase, corresponding to the negative thermal-expansion phenomenon. *catena*-μ-Bromobis(ethylenediamine)platinum(II,IV) diperchlorate, $[Pt(C_2H_8N_2)_2][PtBr_2(C_2H_8N_2)_2](ClO_4)_4$, M_r = 1188.16, λ(Mo $K\alpha$) = 0.71073 Å; low-temperature form, 298 K, monoclinic, $P2_1/m$, a = 8.544 (1), b = 10.973 (1), c = 7.972 (1) Å, β = 109.39 (1)°, V = 705.0 (2) Å^3, Z = 1, D_x = 2.799 Mg m^{-3}, μ = 13.89 mm^{-1}, $F(000)$ = 558, R = 0.029 for 1847 observed reflections [$|F_o| > 3\sigma(F_o)$]; high-temperature form, 298 K, orthorhombic, *Icma*, a = 13.563 (2), b = 10.939 (3), c = 9.664 (2) Å, V = 1433.9 (5) Å^3, Z = 2, D_x = 2.752 Mg m^{-3}, μ = 13.66 mm^{-1}, $F(000)$ = 1116, R = 0.023 for 769 observed reflections [$|F_o| > 3\sigma(F_o)$].

* To whom correspondence should be addressed. Present address: Department of Materials Science, Himeji Institute of Technology, Harima Science Park City, Kamigori-cho, Hyogo 678-12, Japan.

0108-7681/93/030497-10$06.00

1. Introduction

The series of halogen-bridged M^{II}—X—M^{IV} mixed-valence complexes (M = Pt, Pd, Ni; X = Cl, Br, I) have attracted much interest from solid-state physicists and chemists as low-dimensional materials having strong electron-lattice interactions. They have typical Peierls-distorted quasi-one-dimensional structures (Keller, 1982) and show characteristic physical properties such as strong intervalence charge-transfer absorption and luminescence with large Stokes shifts (Tanino & Kobayashi, 1983; Wada, Mitani, Yamashita & Koda, 1985; Wada, Mitani, Toriumi & Yamashita, 1989), and resonance Raman scattering with high overtone progression (Clark & Kurmoo, 1983; Clark, 1984; Tanaka, Kurita, Okada, Kojima & Yamada, 1985). Characteristic phenomena relating to the kink-soliton and polaron have also been observed in these complexes (Kuroda, Sakai, Nishina, Tanaka & Kurita, 1987; Kurita, Haruki & Miyagawa, 1988; Kurita & Haruki, 1989; Haruki & Kurita, 1989; Matsushita, Kojima, Watanabe & Ban, 1989). The solid-state properties can be interpreted by using an extended Peierls–Hubbard model (Nasu, 1983, 1984*a*,*b*; Wada *et al.*, 1985). Recently, we succeeded in the syntheses of novel halogen-bridged Ni^{III}—X—Ni^{III} compounds, $\{[Ni(R,R\text{-chxn})_2X]X_2\}_\infty$ [X = Cl, Br; R,R-chxn = (1R,2R)-cyclohexanediamine], and reported a linear-chain structure with no Peierls distortion, which is an extreme limit of the M^{II}—X—M^{IV} mixed-valence structure (Toriumi, Wada, Mitani, Bandow, Yamashita & Fujii, 1989; Toriumi, Okamoto, Mitani, Bandow, Yamashita, Wada, Fujii, Clark, Michael, Edward, Watkin, Kurmoo & Day, 1990).

In the M^{II}—X—M^{IV} mixed-valence complexes, square-planar four-coordinate $M^{II}(AA)_2$ and octahedral six-coordinate $M^{IV}X_2(AA)_2$ units are stacked alternately, constructing linear chains with an $\cdots M^{II}\cdots X$—M^{IV}—$X\cdots$ repeating unit, where AA denotes a diamine ligand such as ethylenediamine. The positively charged Pt^{II} and Pt^{IV} units are linked by charge-transfer interaction through the bridging halogen ions. The hydrogen bonds between the Pt^{II} and Pt^{IV} units *via* the counter perchlorate ions also play an important role in supporting the linear chain (Toriumi, Yamashita, Ito & Ito, 1986). Recently, remarkable phenomena have been observed for $[Pt(NH_3)_4][PtX_2(NH_3)_4](HSO_4)_4$ (X = Cl, Br), in which lattice parameters along the linear chains decrease monotonically with increasing temperature (Tanaka, Tsujikawa, Toriumi & Ito, 1982). Similar phenomena have been also observed by measuring the shifts of charge-transfer absorption edges with temperature (Matsushita, Kojima, Ban & Tsujikawa, 1989). The negative thermal-expansion phenomena have been interpreted theoretically on the basis of the valence fluctuation of mixed-valence states (Murao, 1987).

In order to elucidate the role of hydrogen-bond networks in these phenomena, we chose the series of complexes $[M(en)_2][MX_2(en)_2](ClO_4)_4$ (M = Pt, Pd; X = Cl, Br, I) since their structures and solid-state properties had been extensively studied. We report here the first-order phase transitions of $[M(en)_2][MX_2(en)_2](ClO_4)_4$ (M = Pt, Pd; X = Cl, Br) which show negative thermal-expansion phenomena around the transition temperatures, the structural analyses of $[Pt(en)_2][PtBr_2(en)_2](ClO_4)_4$ immediately before and after the transition, and the contribution of hydrogen bonds to the phenomena. Hereafter the mixed-valence complexes of $[M(en)_2][MX_2(en)_2](ClO_4)_4$ (M = Pt, Pd; X = Cl, Br, I) are abbreviated as 'MX'.

2. Experimental

Preparation of the samples

The mixed-valence complexes of 'PtX' (X = Cl, Br, I) and 'PdX' (X = Cl, Br) were synthesized by similar methods to those described previously (Matsumoto, Yamashita & Kida, 1978). Crystals were grown from perchloric acid solutions. Single crystals of the monoclinic (low-temperature) and orthorhombic (high-temperature) phases of 'PtBr' used for X-ray analyses were carefully prepared by standing the solutions at 288–293 and 298–303 K, respectively.

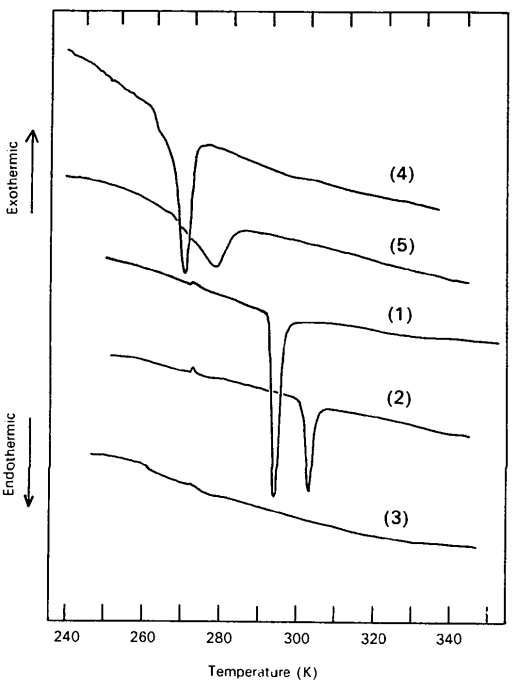

Fig. 1. Results of the differential scanning calorimetric measurements for $[M(en)_2][MX_2(en)_2](ClO_4)_4$: (1) 'PtCl', (2) 'PtBr', (3) 'PtI', (4) 'PdCl' and (5) 'PdBr'.

DSC measurements

Differential scanning calorimetric (DSC) measurements for all the complexes were made with a Du Pont 990 differential scanning calorimeter. Samples of 5–10 mg sealed in aluminium vessels were used for the measurements. The scanning rate was 5 K min^{-1}. Results of the DSC measurements are shown in Fig. 1. For all the complexes except 'PtI', endothermic peaks were observed in the temperature range 269–303 K.

Temperature dependence of the Raman spectra

The Raman spectra were recorded in the backward-scattering configuration, with the incident light polarized parallel to the chain axis of the specimen. The scattered light was analyzed with a double monochromator grating and a photon-counting system. Incident radiation was provided by an Ar-ion laser. The power of the radiation was kept lower than 0.2 mW in order to prevent deterioration of the specimen. Single crystals were used for the measurements. The temperature was controlled in the range 282–313 K with an accuracy of ±0.2 K by using a thermistor.

Temperature dependence of the lattice parameters

The lattice parameters of 'PtX' (X = Cl, Br, I) and 'PdCl' were measured at variable temperatures in the range 123–393 K on the diffractometer with Mo $K\alpha$ radiation (0.71073 Å). The measurement of 'PdBr' failed since the single crystal deteriorated on phase transition. The samples were cooled down and warmed up using a variable-temperature apparatus with a cold nitrogen-gas stream. The temperature was measured with an alumel–chromel thermocouple placed at the same position as that which had been occupied by the sample. Temperature fluctuations were less than ±0.5 K. Accurate lattice parameters were determined by least-squares refinement based on θ values in the range $20 < 2\theta < 30°$: 30 reflections for 'PtCl', 25 for 'PtBr', 25 for 'PtI', and 22 for 'PdCl'. Dimensions of the crystal specimens were: 0.16 × 0.14 × 0.08 mm for 'PtCl', 0.17 × 0.10 × 0.024 mm for 'PtBr', 0.22 × 0.14 × 0.02 mm for 'PtI', and 0.32 × 0.14 × 0.10 mm for 'PdCl'.

In order to confirm the transition temperatures and the hysteresis phenomena, variations of the Bragg positions and intensities with temperature were carefully monitored in the region of the transition temperatures for seven strong reflections. The reversibility of the phase-transition phenomena was also confirmed by repeating the measurements.

X-ray data collection

Intensity data for both the monoclinic and orthorhombic phases of 'PtBr' were measured at room temperature (298 K) on a Rigaku AFC-5 diffractometer, graphite-monochromated Mo $K\alpha$ radiation, θ–2θ scan technique, scan rate 3° min^{-1}, scan range $(1.3 + 0.5\tan\theta)°$. For the monoclinic phase, conditions for the data collection were: lustrous green square prism with (010) elongated; crystal dimensions 0.37 × 0.20 × 0.15 mm; $2\theta_{max} = 65°$; h 0 to 12, k 0 to 16, l −12 to 12; 2822 reflections measured; 1847 reflections with $|F_o| > 3\sigma(F_o)$ observed; $R_{int} = 0.0175$ for 97 symmetry-related pairs. For the orthorhombic phase: lustrous green square plate with (010) developed; crystal dimensions 0.24 × 0.19 × 0.06 mm; $2\theta_{max} = 60°$; h −19 to 19, k 0 to 14, l 0 to 13; 2311 reflections measured; 769 reflections with $|F_o| > 3\sigma(F_o)$ observed; $R_{int} = 0.0185$ for 695 symmetry-related pairs. Three standard reflections monitored every 50 reflections showed no crystal movement or decay. Intensity corrected by numerical absorption method based on Gaussian integration, transmission-factor ranges for the monoclinic and orthorhombic phases were 0.1813–0.0321 and 0.4429–0.1128, respectively. Accurate cell parameters for the monoclinic and orthorhombic phases were determined by least-squares fit for 48 reflections ($25 < 2\theta < 30°$) and 26 reflections ($25 < 2\theta < 30°$) measured on the diffractometer.

3. Structure analyses

Structure analyses of 'PtBr' have already been reported for the orthorhombic phase (Endres, Keller, Martin, Traeger & Novotny, 1980), and more recently for both the monoclinic and orthorhombic phases (Keller, Müller, Ledezma & Martin, 1985). Keller *et al.* adopted the noncentrosymmetric space groups $P2$ and $Ic2a$, instead of the plausible centrosymmetric $P2_1/m$ and $Icma$, for the monoclinic and orthorhombic phases, respectively. The molecular structure of the $Pt(en)_2$ unit reported in the monoclinic phase seems to be unusual compared with those of the analogous Pd complexes (Beauchamp, Layek & Theophanides, 1982; Yamashita, Toriumi & Ito, 1985).

Systematic absences (for the monoclinic phase, $k = 2n$ for $0k0$; for the orthorhombic phase, $h + k + l = 2n$ for hkl; h, $k = 2n$ for $hk0$; k, $l = 2n$ for $0kl$) indicate the possible space groups $P2_1$ or $P2_1/m$ for the monoclinic form, and $Ic2a$ or $Icma$ for the orthorhombic form, respectively. Crystal structure analyses were successfully carried out by adopting the centrosymmetric space groups $P2_1/m$ and $Icma$ for the monoclinic and orthorhombic phases, respectively.

The structures were solved by a conventional heavy-atom method, and refined on F by a full-matrix least-squares technique. All the non-H atoms were refined anisotropically. H atoms were located

by difference syntheses and refined isotropically. Positional disorders of the bridging Br atoms were found for both the monoclinic and orthorhombic phases. For the orthorhombic phase, an orientational disorder of the perchlorate ion was also observed and included in the refinement. Isotropic secondary-extinction corrections were applied to both refinements: secondary-extinction coefficients g and minimum-extinction factors were $2.5\ (2) \times 10^{-5}$ and 0.59 for the monoclinic form, and $2.1\ (1) \times 10^{-4}$ and 0.60 for the orthorhombic form, respectively. For the monoclinic form, $R(F) = 0.029$, $wR(F) = 0.036$, $S = 1.30$ for 1847 independent reflections, weighting scheme $w = [\sigma_c^2 + (0.020|F_o|)^2]^{-1}$, 139 parameters refined, maximum and minimum peak heights in the difference Fourier map are 2.3 and -2.7 e Å^{-3} (around the Br atom), $(\Delta/\sigma)_{max} = 0.10$. For the orthorhombic form, $R(F) = 0.023$, $wR(F) = 0.027$, $S = 1.23$ for 769 independent reflections, $w = [\sigma_c^2 + (0.015|F_o|)^2]^{-1}$, 83 parameters refined, maximum and minimum peak heights in the difference Fourier map are 0.5 and -0.7 e Å^{-3}, $(\Delta/\sigma)_{max} = 0.25$. Atomic scattering factors and anomalous-scattering corrections were taken from *International Tables for X-ray Crystallography* (1974, Vol. IV). Atomic parameters for the monoclinic and orthorhombic phases are listed in Table 1.*

All the calculations were carried out on a HITAC M680H computer at the Computer Center of the Institute for Molecular Science with *UNICS*III (Sakurai & Kobayashi, 1979), full-matrix least-squares program *RADIEL* (Coppens, Guru Row, Leung, Stevens, Becker & Yang, 1979) and *ORTEP* (Johnson, 1965).

Table 1. *Fractional coordinates* ($\times 10^4$) *and equivalent isotropic thermal parameters* (Å^2) *for non*-H *atoms of* $[Pt(en)_2][PtBr_2(en)_2](ClO_4)_4$

$B_{eq} = (4/3)\sum_i\sum_j \beta_{ij}\mathbf{a}_i.\mathbf{a}_j$.

	x	y	z	B_{eq}
(*a*) Monoclinic (low-temperature) phase				
Pt	0	0	0	1.33
Br*	36 (2)	2263 (1)	−143 (2)	2.07
N(1)	2411 (6)	−56 (4)	36 (6)	2.01
N(2)	1082 (6)	50 (5)	2713 (6)	2.07
C(1)	3506 (8)	341 (7)	1834 (9)	2.61
C(2)	2879 (8)	−247 (6)	3191 (8)	2.55
Cl(1)	2796 (3)	2500	6391 (3)	2.49
Cl(2)	−2620 (3)	2500	3156 (3)	2.25
O(11)	2089 (9)	1439 (5)	6855 (9)	5.25
O(12)	2461 (11)	2500	4501 (9)	4.01
O(13)	4540 (12)	2500	7294 (14)	6.59
O(21)	−1612 (8)	1429 (4)	3624 (8)	4.05
O(22)	−3825 (9)	2500	4049 (9)	3.44
O(23)	−3462 (9)	2500	1252 (9)	3.47
(*b*) Orthorhombic (high-temperature) phase				
Pt	0	2500	0	1.61
Br*	0	239 (1)	0	2.63
N	1007 (4)	2475 (5)	1593 (5)	2.76
C	474 (6)	2794 (6)	2913 (7)	3...8
Cl	2981 (2)	5000	796 (3)	3.56
O(1)	2627 (5)	3928 (5)	184 (6)	5.97
O(2)*	4070 (15)	5000	317 (24)	5.59
O(3)*	2997 (31)	5000	2201 (21)	8.87
O(2')*	3864 (20)	5000	1406 (57)	10.56
O(3')*	2242 (25)	5000	1925 (24)	13.04

* Occupancies for the disordered atoms are 0.5.

4. Results and discussion

Phase transition

The temperature dependence of the lattice parameters for all the complexes except for 'PdBr' is shown in Fig. 2. Both the temperature dependence of the lattice parameters and the DSC measurements revealed the first-order phase transitions of 'MX' (M = Pt, Pd; X = Cl, Br). The phase-transition temperatures were determined by the measurements of temperature dependence of the lattice parameters: 293.2 K for 'PtCl', 297.8 K for 'PtBr', and 269.3 K for 'PdCl', respectively. The transition temperature of 279 K for 'PdBr' was obtained from the DSC measurement, since the crystal deteriorated at the phase transition. Small hysteresis phenomena (about 2 K) and their reversibility have been confirmed by measuring the temperature dependences of both the positions and intensities of Bragg spots. Keller *et al.* (1985) reported a similar phase-transition phenomenon for 'PtBr', though they claimed that the transition occurred as a result of X-ray irradiation. Fig. 3 shows the temperature dependence of the ν(Pt—Cl) band on the Raman scattering of 'PtCl'. The phase-transition temperatures for 'PtCl' determined by the three methods are consistent with each other.

The space groups of all the complexes are summarized in Table 2. The space group of 'PtI' is different from those of the other crystals, consistent with the difference in thermal behavior. The similarity in both the crystal structures and the phase-transition behavior of 'MX' (M = Pt, Pd; X = Cl, Br) strongly suggests that the same type of phase transitions occurred in all the crystals except for 'PtI'. It should be noted that the lattice parameters along the linear chains (b axis) show negative thermal-expansion phenomena at the phase-transition temperatures. This will be discussed later.

Crystal and linear-chain structures of the monoclinic (low-temperature) and orthorhombic (high-temperature) phases

Relevant interatomic distances and angles are presented in Table 3. Fig. 4 shows the crystal structures of the monoclinic and orthorhombic phases viewed along infinite chains of the b axes. The crystal struc-

* Lists of structure factors, anisotropic thermal parameters and H-atom parameters have been deposited with the British Library Document Supply Centre as Supplementary Publication No. SUP 55826 (17 pp.). Copies may be obtained through The Technical Editor, International Union of Crystallography, 5 Abbey Square, Chester CH1 2HU, England. [CIF reference: AS0410]

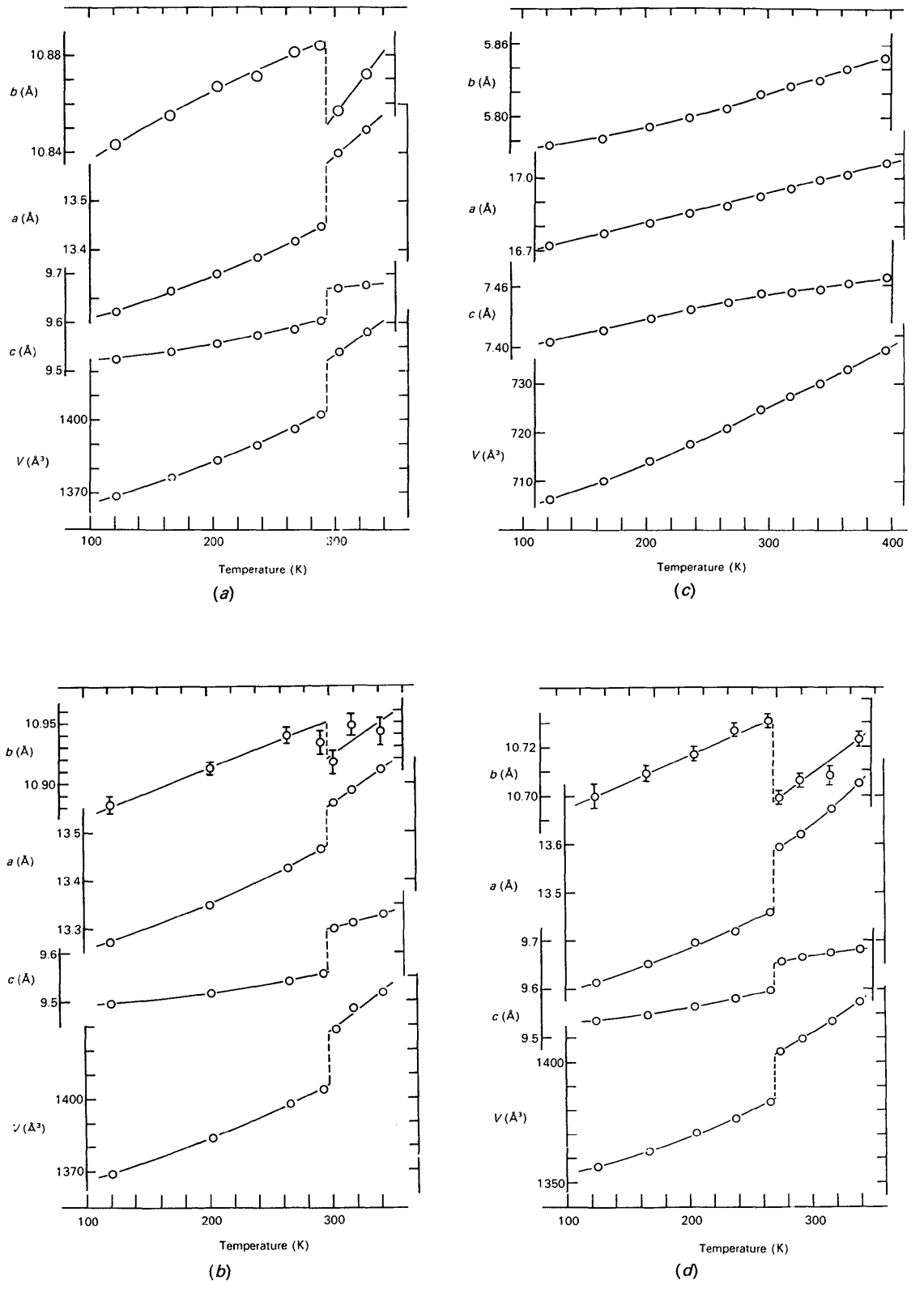

Fig. 2. Variation with temperature of the lattice parameters for $[M(en)_2][MX_2(en)_2](ClO_4)_4$: (*a*) 'PtCl', (*b*) 'PtBr', (*c*) 'PtI' and (*d*) 'PdCl'. The e.s.d.'s are smaller than the plotted circles or are given by the vertical lines.

ture of the orthorhombic phase is isomorphous with those of the analogous Pd^{II}—X—Pd^{IV} complexes, $[Pd(en)_2][PdCl_2(en)_2](ClO_4)_4$ (Beauchamp *et al.*, 1982) and $[Pd(en)_2][PdBr_2(en)_2](ClO_4)_4$ (Yamashita *et al.*, 1985). Recently, the monoclinic structure of $[Pt(en)_2][PtBr_2(en)_2](ClO_4)_4$, which was crystallized under high pressure, has been reported (Weinrach, Ekberg, Conradson, Swanson & Hochheimer, 1990). The reported monoclinic cell seems to be reduced into the *C*-centered orthorhombic cell having the same lattice parameters as this orthorhombic phase. Although the monoclinic structure is almost the same as the orthorhombic one, there are some remarkable differences as discussed below.

Perspective views of portions of the infinite linear chains for the monoclinic and orthorhombic phases are shown in Fig. 5. The monoclinic and orthorhombic phases contain linear chains and perchlorate anions, respectively. The chain structure, which is exactly linear in the orthorhombic phase, is clearly bent in the monoclinic phase. The 'bend' angle defined by the Pt—Br bond and the *b* axis is 2.94 (3)°. As shown in Fig. 4, the perchlorate ions are ordered in the monoclinic phase, but are disordered in the orthorhombic phase as observed for the analogous complexes (Beauchamp *et al.*, 1982; Yamashita *et al.*, 1985).

The crystallographically independent Pt complexes lie in particular positions: 222 in the orthorhombic and $\bar{1}$ in the monoclinic phase, respectively. The Pt atoms are surrounded by four N atoms of two ethylenediamine ligands in a square-planar fashion. The average Pt—N distances for the monoclinic and orthorhombic phases are 2.051 (3) and 2.058 (5) Å, respectively. Two five-membered chelate rings adopt the most stable *gauche* conformation: the absolute conformations are $\lambda\lambda$ or $\delta\delta$ in the orthorhombic phase and $\lambda\delta$ or $\delta\lambda$ in the monclinic phase. Although the $\lambda\lambda$ or $\delta\delta$ conformation is usually observed, the $\lambda\delta$ or $\delta\lambda$ conformation is occasionally found. In each phase, neighboring $Pt(en)_2$ moieties on the chain are related by the mirror planes which

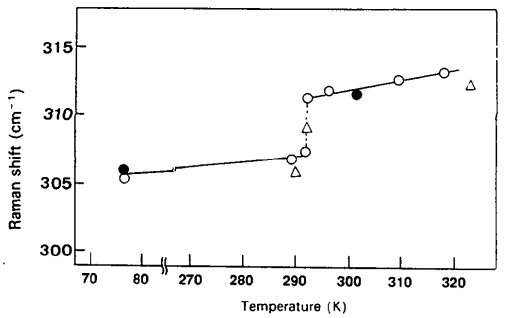

Fig. 3. Variation with temperature of the ν(Pt—Cl) band in the Raman spectra of $[Pt(en)_2][PtCl_2(en)_2](ClO_4)_4$: excitation lines are 514.5 (○), 501.7 (△), and 488.0 nm (●).

Table 2. *Crystal data of* $[M^{II}(en)_2][M^{IV}X_2(en)_2](ClO_4)_4$ *(abbreviated as 'MX')*

	'PtCl'	'PtBr'	'PtI'	'PdCl'	'PdBr'
Crystal system	Orthorhombic	Orthorhombic	Monoclinic	Orthorhombic	Orthorhombic
a (Å)	13.525 (2)	13.563 (2)	17.031 (10)	13.636 (3)	13.608 (2)
b (Å)	10.807 (2)	10.939 (3)	5.827 (4)	10.715 (7)	10.814 (1)
c (Å)	9.643 (1)	9.664 (2)	7.440 (4)	9.665 (2)	9.663 (4)
β (°)	–	–	97.93 (4)	–	–
V (Å^3)	1409.4	1433.9 (5)	731.3	1412.2 (10)	1422.0 (3)
Space group	*Icma*	*Icma*	*C2/m*	*Icma*	*Icma*
Z	2	2	1	2	2
References	(1)	This work	(2)	(3)	(4)*

References: (1) Matsumoto, Yamashita, Ueda & Kida (1978). (2) Endres, Keller, Martin, Gung & Traeger (1979). (3) Beauchamp, Layek & Theopanides (1982). (4) Yamashita, Toriumi & Ito (1985).

* Martin, Keller & Müller (1985) reported the structural analysis of the same crystal, but adopted the noncentrosymmetric space group *Ic2a* instead of the correct *Icma*.

Table 3. *Interatomic distances* (Å) *and angles* (°) *of* $[Pt(en)_2][PtBr_2(en)_2](ClO_4)_4$

	Monoclinic phase	Orthorhombic phase	Difference
Pt—Br	2.487 (1)	2.473 (1)	−0.014 (1)
Pt···Br', Br''*	3.006 (1)	2.996 (1)	−0.010 (1)
Pt—N(1), N(1^{iii})*	2.051 (5)	2.058 (5)	+0.007 (6)
Pt—N(2)	2.051 (4)	–	
N(1)—C(1)	1.493 (8)	1.508 (9)	
N(2)—C(2)	1.490 (8)	–	
C(1)—C(2), C(2^{iii})*	1.503 (11)	1.438 (12)	
Br—Pt—N(1)	90.2 (1)	89.2 (2)	
Br—Pt—N(2)	90.8 (1)	–	
N(1)—Pt—N(2), N(1^{iii})*	83.5 (2)	83.2 (2)	
Pt—N(1)—C(1)	108.1 (4)	108.2 (4)	
Pt—N(2)—C(2)	109.2 (4)	–	
N(1)—C(1)—C(2), C(1^{iii})*	107.8 (5)	109.0 (6)	
N(2)—C(2)—C(1)	107.8 (5)	–	
Cl(1)—O(11), O(1)*	1.417 (7)	1.399 (6)	
Cl(1)—O(12), O(2)*†	1.437 (8)	1.547 (21)	
Cl(1)—O(13), O(3)*‡	1.424 (9)	1.358 (21)	
Cl(2)—O(21)	1.432 (5)	–	
Cl(2)—O(22)	1.433 (9)	–	
Cl(2)—O(33)	1.448 (7)	–	

Symmetry codes: (i) $-x, -\frac{1}{2}+y, -z$; (ii) $-x, -y, -z$; (iii) $-x, \frac{1}{2}-y, z$.

* Where alternative atoms are given, the first atom refers to the monoclinic phase and the second to the orthorhombic phase.
† The Cl(1)—O(2′) distance is 1.334 (34) Å.
‡ The Cl(1)—O(3′) distance is 1.482 (29) Å.

are perpendicular to the chain and pass through the midpoint between two Pt units. The bridging Br atom is positionally disordered at two positions equidistant from the midpoint between two Pt atoms with an occupancy factor of 0.5. These positions are 0.520 (1) Å apart for the monoclinic structure and 0.523 (2) Å apart for orthorhombic structure.

Keller *et al.* (1985) made a X-ray photographic studies of 'PtBr' and observed diffuse scattering corresponding to the commensurate linear-chain structure with a ···Pt^{II}···Br—Pt^{IV}—Br··· repeating unit. In the mixed-valence complex, the square-planar four-coordinate Pt^{II} and the octahedral six-coordinate Pt^{IV} units are stacked alternately to construct the chain structure. Because of the positional disorder of the bridging Br atom, which corresponds to a non-periodic arrangement of the Pt^{II} and Pt^{IV} units in the **ac** plane, the oxidation states of the Pt atoms cannot

be identified. There are two Pt—Br distances along the chain. The shorter one corresponds to the Pt^{IV}—Br distance and the longer one to the $Pt^{II}\cdots Br$ separation. The ratios of the Pt^{IV}—Br to $Pt^{II}\cdots Br$ distances in the monoclinic and orthorhombic phases are 0.827 and 0.825, respectively.

As has been observed for the analogous mixed-valence complexes, the neighboring $Pt(en)_2$ moieties on the chain are linked by hydrogen-bond chains involving perchlorate ions, NH···O(perchlorate)···HN. The hydrogen-bond chains play an important role in constructing the linear-chain structure, and in determining the structural parameters along the chain (Toriumi *et al.*, 1986). The hydrogen-bond distances in the monoclinic and orthorhombic phases are summarized in Table 4. It should be noted that a remarkable change in the hydrogen-bond network occurred together with the conformational change of the ethylenediamine chelate rings, which will be described in detail in the next section.

Structural changes between the monoclinic and orthorhombic phases on phase transition

The relationships between the monoclinic (a_m, b_m and c_m) and orthorhombic cells (a_o, b_o and c_o) are

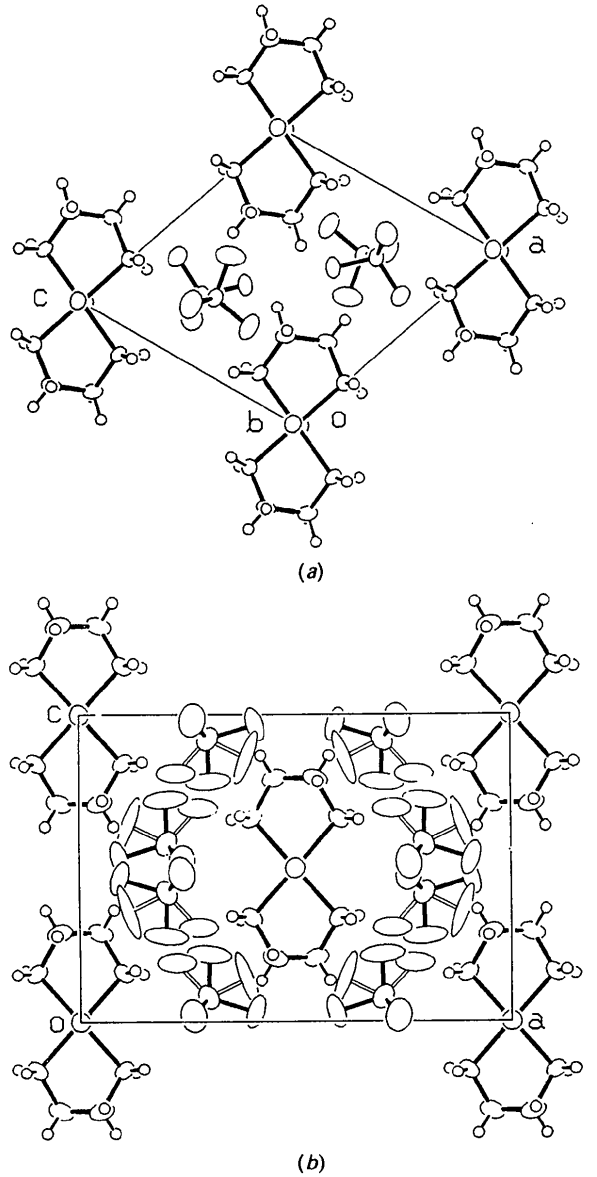

Fig. 4. Perspective views of the crystal structures of $[Pt(en)_2][PtBr_2(en)_2](ClO_4)_4$ viewed along the b axes: (*a*) monoclinic phase, (*b*) orthorhombic phase. Disordered perchlorate O atoms are depicted by ellipsoids attached to the rod or pipe bonds.

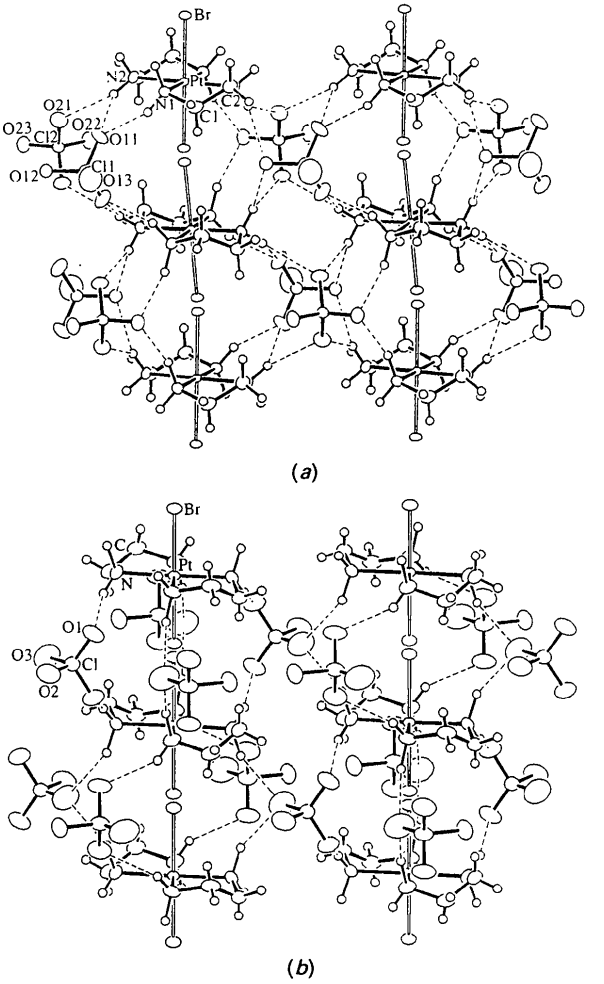

Fig. 5. *ORTEP* drawings of portions of the infinite chains of $[Pt(en)_2][PtBr_2(en)_2](ClO_4)_4$ along the b axes with surrounding ClO_4^- ions and the closest neighboring chain, showing atomic numbering schemes; thermal ellipsoids at the 40% probability level, hydrogen bonds shown by broken lines: (*a*) monoclinic (low-temperature) phase, (*b*) orthorhombic (high-temperature) phase. Bridging Br atoms are disordered at two positions equidistant from two Pt atoms with populations of 0.5. Disordered perchlorate O atoms in the orthorhombic phase are omitted for clarity.

Table 4. *Hydrogen-bond distances* (Å) *of* $[Pt(en)_2][PtBr_2(en)_2](ClO_4)_4$

	H···O	N···O
(*a*) Monoclinic (low-temperature) phase		
N(1)—H(1)···O(11')	2.01 (9)	2.955 (8)
N(1)—H(2)···O(23ⁱⁱ)	2.10 (8)	3.109 (7)
N(2)—H(3)···O(11ⁱⁱⁱ)	2.48 (8)	3.278 (10)
N(2)—H(3)···O(21)	2.45 (7)	3.037 (9)
N(2)—H(4)···O(12)	2.32 (7)	3.087 (6)
N(2)—H(4)···O(21ⁱⁱⁱ)	2.44 (9)	3.239 (8)
(*b*) Orthorhombic (high-temperature) phase		
N—H(2)···O(1)	2.26 (8)	3.034 (8)
N—H(1)···O(3ᵛ)	2.23 (7)	3.243 (20)
N—H(2)···O(3ᵛⁱ)	2.39 (8)	3.246 (19)

Symmetry codes: (i) $x, y, -1+z$; (ii) $-x, -\frac{1}{2}+y, -z$; (iii) $-x, -y, 1-z$; (iv) $\frac{1}{2}-x, \frac{1}{2}+y, \frac{1}{2}-z$; (v) $x, 1-y, z$.

shown in Fig. 6. These are given as: $a_o = a_m - c_m$, $b_o = b_m$ and $c_o = a_m + c_m$ in real space; $a_o^* = \frac{1}{2}(a_m^* - c_m^*)$, $b_o^* = b_m^*$ and $c_o^* = \frac{1}{2}(a_m^* + c_m^*)$ in reciprocal space. The b or b^* axis is common for both the cells in real or reciprocal space, respectively.

Comparing the symmetry operations of the monoclinic and orthorhombic cells carefully, it has become apparent that the differences between the space groups $P2_1/m$ and *Icma* can be expressed as the conversion of site symmetry at the Pt complexes from $\bar{1}$ in the monoclinic to 222 in the orthorhombic form. Alternatively, the mirror plane by which neighboring $Pt(en)_2$ moieties on the chain are related remains unchanged. The drastic change of site symmetry is a result of the interconversion of the chelate-ring conformations of $Pt(en)_2$ moieties. The square-planar $[Pt^{II}(en)_2]^{2+}$ or octahedral $[Pt^{IV}Br_2(en)_2]^{2+}$ complex with the chelate-ring conformations $\lambda\lambda$ or $\delta\delta$ has the molecular symmetry 222 and that with $\lambda\delta(\delta\lambda)$ only $\bar{1}$. This structural change is clearly demonstrated by the schematic drawing shown in Fig. 7, in which only the chelate-ring conformations of $Pt(en)_2$ moieties are emphasized for clarity. Taking into account the chelate-ring conformations only, the chain structures can be expressed as the sequence $\cdots(\delta\lambda)(\lambda\delta)(\delta\lambda)(\lambda\delta)\cdots$ for the monoclinic structure and $\cdots(\lambda\lambda)(\delta\delta)(\lambda\lambda)(\delta\delta)\cdots$ for the orthorhombic structure. It should be noted that one of the two

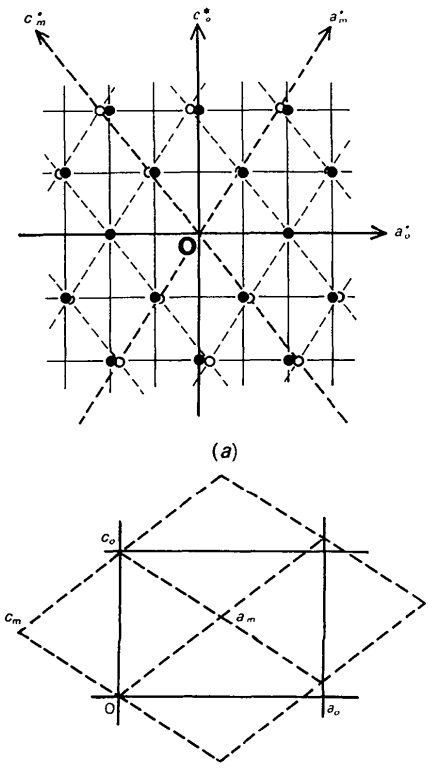

Fig. 6. Relationship between the monoclinic (low-temperature) and orthorhombic (high-temperature) cells: (*a*) reciprocal space, (*b*) real space. The monoclinic and orthorhombic cells are expressed by the subscripts *m* and *o*, respectively. The b^* or b axis is common for both the cells.

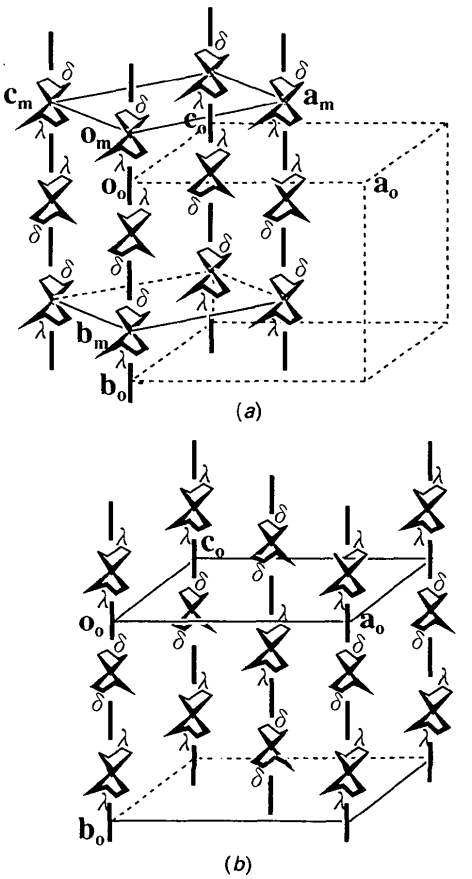

Fig. 7. Schematic drawings of the crystal structure: (*a*) monoclinic cell and (*b*) orthorhombic cell. Only the chelate-ring conformations of $Pt(en)_2$ moieties are depicted, perchlorate anions being omitted for clarity. Bold lines along the b axes indicate the linear-chain structures, and solid and broken lines the monoclinic and orthorhombic cells, expressed by the subscripts *m* and *o*, respectively.

chelate-ring conformations is changed in each $Pt(en)_2$ moiety on phase transition. The correlations of the chelate-ring conformations among chains are also different. Although all the conformational sequences among the chains are the same in the monoclinic form, those in the orthorhombic form are shifted by half a repeating unit from the closest neighboring chains. This inter-chain correlation may depend on the hydrogen bonds between chains *via* counter anions. These intra- and inter-chain structural changes relating to the conformational changes of $Pt(en)_2$ moieties may result in the drastic change of the unit cell from the primitive monoclinic cell of $P2_1/m$ to the body-centered orthorhombic cell of *Icma*.

As described in the previous section, the linear chain is slightly bent in the monoclinic cell although it is exactly linear in the orthorhombic cell. This can be interpreted simply from the crystallographic point of view that there is no symmetrical constraint on the chain structure in the monoclinic cell but the chain in the orthorhombic cell lies on the twofold axis. In other words, the arrangement of perchlorate ions around the linear chain is non-symmetrical in the monoclinic form but has twofold symmetry to be linear in the orthorhombic form. This difference should also be coupled with the interconversion of the chelate-ring conformations of $Pt(en)_2$ moieties, since the Pt complexes are linked by hydrogen bonds between the NH groups of the ethylenediamine ligands through the perchlorate ions as described previously. Fig. 8 shows schematic drawings of the interchain hydrogen bonds in the monoclinic and orthorhombic cells. The hydrogen-bond network in the monoclinic phase is extended two-dimensionally along the **bc** plane, and that in the orthorhombic phase is three-dimensional. Comparing the hydrogen-bond distances for both phases, it has become apparent that the hydrogen-bond network in the monoclinic phase is stronger than those in the orthorhombic phase. The order–disorder transformation of the perchlorate ion has been observed but could not yet be explained.

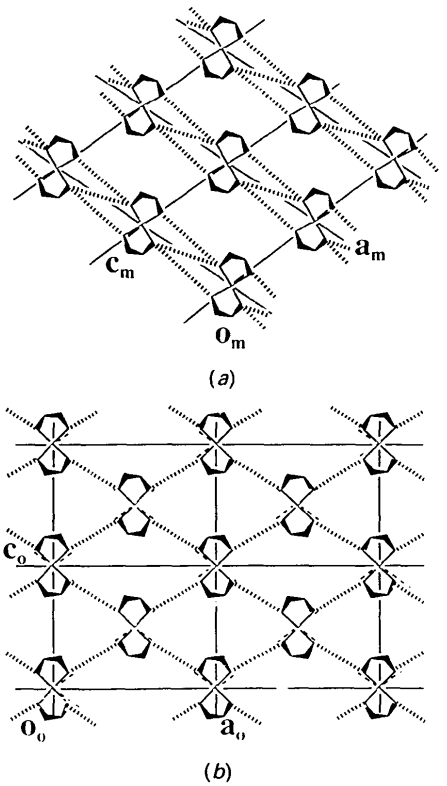

Fig. 8. Schematic drawings of the hydrogen-bond networks between chains, showing hydrogen bonds as broken lines, chelate-ring conformations of $Pt(en)_2$ moieties: (*a*) monoclinic cell and (*b*) orthorhombic cell. Perchlorate ions are omitted for clarity.

Considering the structural changes described above, it can be presumed that the increase of lattice vibrations, especially the increase of thermal motions of both the ethylenediamine chelate rings and the perchlorate ions, partly destroys the hydrogen-bond network, leading to the phase transition from the monoclinic to the orthorhombic phase with high symmetry. This assumption may be supported by the result that the transition temperatures increase as the molecular weights of the complexes increase: 'PdCl' < 'PdBr' < 'PtCl' < 'PtBr'.

Negative thermal expansion along the chain structure

Negative thermal-expansion phenomena around the transition temperatures have been observed for all the complexes except for 'PtI'. Fig. 2 shows that, as the temperature increases, the lattice parameters along the chains (*b* axes) decrease discontinuously in the vicinity of the phase-transition temperatures, although *a*, *c* and *V* increase normally. These abnormal phenomena can be considered as characteristic features of the linear-chain structures, because these complexes are essentially quasi-one-dimensional materials.

Comparing the structural parameters in Table 3, both the Pt^{IV}—Br and $Pt^{II}\cdots Br$ distances of the monoclinic phase are significantly elongated [by 0.014 (1) and 0.010 (1) Å] compared to those of the orthorhombic phase. The Pt—N distance of the monoclinic phase is, however, shorter than that of the orthorhombic phase.

As discussed in the preceding section, the neighboring $Pt(en)_2$ units on the chain are linked by the hydrogen-bond chains *via* perchlorate ions. The hydrogen bonds in the monoclinic phase are stronger than those in the orthorhombic phase. In addition, the linear-chain structure in the monoclinic phase is

slightly bent, though that in the orthorhombic phase is exactly linear. These facts tend to shrink the Pt···Pt separation in the monoclinic phase, which corresponds to a normal thermal-expansion phenomenon.

This abnormal phenomenon seems to be well interpreted on the basis of the change in in-plane ligand field strength around the Pt^{II} and Pt^{IV} atoms owing to the change in the hydrogen-bond strength. As the strength of the N—H···O(ClO_4^-) hydrogen bonds increases, polarization of the N—H bond increases. This increases the net charges of the ligating N atoms. It appears consistent with this explanation that the Pt—N distance in the orthorhombic phase is slightly longer than that in the monoclinic phase. Thus, the increase of hydrogen-bond strength may cause the increase of in-plane ligand field strength, resulting in the elongation of axial Pt^{IV}—X and Pt^{II}···X bond distances. By measuring the pressure dependences of IR spectra of the halogen-bridged linear-chain compounds {[M(R,R-chxn)$_2$Br]Br$_2$} (M = Pt, Pd, Ni), the strong correlation between the ν(N—H) band of diamine ligands and the oxidation states of metal atoms has been observed (Okaniwa, Okamoto, Mitani, Toriumi & Yamashita, 1991). Consequently, it could be concluded that the hydrgen-bond network between the complex and counter ions makes both electronic and structural contributions to the linear-chain structure (Okamoto, Mitani, Toriumi & Yamashita, 1992).

The effect of valence fluctuations of the metal atoms may also affect this abnormal phenomenon. From the viewpoint of the valence fluctuation, Murao pointed out that the minimization calculation of the free energy of a quasi-one-dimensional $Pt^{3+\delta}$—X—$Pt^{3-\delta}$ system provided the contraction of $Pt^{3-\delta}$—X distance and the expansion of $Pt^{3+\delta}$—X distance with increasing temperature, leading to the overall negative thermal-expansion phenomenon (Murao, 1987). However, both the Pt^{IV}—Br and Pt^{II}···Br distances in the 'PtBr' system contract as temperature increases.

This work was supported in part by a grant-in-aid for Science Research from the Ministry of Education, Science and Culture, Japan.

References

Beauchamp, A. L., Layek, D. & Theophanides, T. (1982). *Acta Cryst.* B**38**, 1158–1164.

Clark, R. J. H. (1984). *Adv. Infrared Raman Spectrosc.* **11**, 95–132.

Clark, R. J. H. & Kurmoo, M. (1983). *J. Chem. Soc. Faraday Trans.* 2, **79**, 519–527.

Coppens, P., Guru Row, T. N., Leung, P., Stevens, E. D., Becker, P. J. & Yang, Y. W. (1979). *Acta Cryst.* A**35**, 63–72.

Endres, H., Keller, H. J., Martin, R., Gung, H. N. & Traeger, U. (1979). *Acta Cryst.* B**35**, 1885–1887.

Endres, H., Keller, H. J., Martin, R., Traeger, U. & Novotny, M. (1980). *Acta Cryst.* B**36**, 35–39.

Haruki, M. & Kurita, S. (1989). *Phys. Rev. B*, **39**, 5706–5712.

Johnson, C. K. (1965). *ORTEP*. Report ORNL-3794. Oak Ridge National Laboratory, Tennessee, USA.

Keller, H. J. (1982). *Linear Chain Platinum Haloamines*. In *Extended Linear Chain Compounds*, Vol. 1, edited by J. S. Miller, pp. 357–407. New York: Plenum Press.

Keller, H. J., Müller, B., Ledezma, G. & Martin, R. (1985). *Acta Cryst.* C**41**, 16–20.

Kurita, S. & Haruki, M. (1989). *Synth. Met.* **29**, F129–F136.

Kurita, S., Haruki, M. & Miyagawa, K. (1988). *J. Phys. Soc. Jpn*, **57**, 1789–1796.

Kuroda, N., Sakai, M., Nishina, Y., Tanaka, M. & Kurita, S. (1987). *Phys. Rev. Lett.* **58**, 2122–2125.

Martin, R., Keller, H. J. & Müller, B. (1985). *Z. Naturforsch. Teil B*, **40**, 57–60.

Matsumoto, N., Yamashita, M. & Kida, S. (1978). *Bull. Chem. Soc. Jpn*, **51**, 2334–2337.

Matsumoto, N., Yamashita, M., Ueda, I. & Kida, S. (1978). *Mem. Fac. Sci. Kyushu Univ. Ser. C*, **11**, 209–216.

Matsushita, N., Kojima, N., Ban, T. & Tsujikawa, I. (1989). *Bull. Chem. Soc. Jpn*, **62**, 3906–3910.

Matsushita, N., Kojima, N., Watanabe, N. & Ban, T. (1989). *Solid State Commun.* **71**, 253–258.

Murao, T. (1987). *Phys. Rev. B*, **35**, 6051–6058.

Nasu, K. (1983). *J. Phys. Soc. Jpn*, **52**, 3865–3873.

Nasu, K. (1984*a*). *J. Phys. Soc. Jpn*, **53**, 302–311.

Nasu, K. (1984*b*). *J. Phys. Soc. Jpn*, **53**, 427–437.

Okamoto, H., Mitani, T., Toriumi, K. & Yamashita, M. (1992). *Mater. Sci. Eng.* B**13**, L9–L14.

Okaniwa, K., Okamoto, H., Mitani, T., Toriumi, K. & Yamashita, M. (1991). *J. Phys. Soc. Jpn.* **60**, 997–1004.

Sakurai, T. & Kobayashi, K. (1979). *Rikagaku Kenkyusho Hokoku*, **55**, 69–77. (In Japanese.)

Tanaka, M., Kurita, S., Okada, Y., Kojima, T. & Yamada, Y. (1985). *Chem. Phys.* **96**, 343–348.

Tanaka, M., Tsujikawa, I., Toriumi, K. & Ito, T. (1982). *Acta Cryst.* B**38**, 2793–2797.

Tanino, H. & Kobayashi, K. (1983). *J. Phys. Soc. Jpn*, **52**, 1446–1456.

Toriumi, K., Okamoto, H., Mitani, T., Bandow, S., Yamashita, M., Wada, Y., Fujii, Y., Clark, R. J. H., Michael, D. J., Edward, A. J., Watkin, D., Kurmoo, M. & Day, P. (1990). *Mol. Cryst. Liq. Cryst.* **181**, 333–342.

Toriumi, K., Wada, Y., Mitani, T., Bandow, S., Yamashita, M. & Fujii, Y. (1989). *J. Am. Chem. Soc.* **111**, 2341–2342.

Toriumi, K., Yamashita, M., Ito, H. & Ito, T. (1986). *Acta Cryst.* C**42**, 963–968.

Wada, Y., Mitani, T., Toriumi, K. & Yamashita, M. (1989). *J. Phys. Soc. Jpn*, **58**, 3013–3021.

Wada, Y., Mitani, T., Yamashita, M. & Koda, T. (1985). *J. Phys. Soc. Jpn*, **54**, 3143–3153.

Weinrach, J. B., Ekberg, S. A., Conradson, S. D., Swanson, B. I. & Hochheimer, H. D. (1990). *Inorg. Chem.* **29**, 981–985.

Yamashita, M., Toriumi, K. & Ito, T. (1985). *Acta Cryst.* C**41**, 876–878.